

# Higher Harmonics of Double White Dwarfs in the Centihertz Band: Linking LISA and DECIGO

Naoki Seto

*Department of Physics, Kyoto University, Kyoto 606-8502, Japan*

(Dated: January 22, 2026)

We investigate the detectability of post-Newtonian higher harmonics from Galactic double white dwarfs in the centihertz band ( $\sim 0.01$  Hz). Using a synthetic population, we show that, unlike the quadrupole mode, higher harmonics remain undetectable with LISA except for rare nearby systems. In contrast, planned mid-band (decihertz) observatories such as DECIGO and BBO will be able to detect the third harmonic for about 10% of inspiral binaries above  $\sim 5$  mHz, enabling statistical constraints on mass ratios. These results highlight the successive roles of LISA and future decihertz missions in establishing a coherent strategy for space-based gravitational-wave astronomy.

## I. INTRODUCTION

Short-period double white dwarfs (DWDs) are numerous sources of low-frequency gravitational waves (GWs) in our Galaxy and represent one of the primary targets for the Laser Interferometer Space Antenna (LISA) [1–7]. Most DWDs are expected to circularize during their evolutionary history, and their quadrupole emission (the fundamental  $k = 2$  harmonic) will be detected from thousands of Galactic systems, providing a nearly complete census of the population above  $\sim 4$  mHz [6]. While the quadrupole mode ensures detections across the Galaxy, it alone does not provide direct information on the binary mass ratio.

Even for circular binaries, higher harmonics arise at post-Newtonian (PN) order and offer a direct probe of mass asymmetry [8–10]. In particular, the first ( $k = 1$ ) and third ( $k = 3$ ) harmonics appear at 0.5PN order with amplitudes proportional to  $\beta\Delta$ , where  $\beta \sim v/c$  is the PN velocity parameter and  $\Delta$  is the fractional mass difference. These harmonics vanish in the equal-mass limit and therefore carry unique information about the distribution of mass ratios in the binaries. Their importance has already been demonstrated for black hole binaries observed with ground-based interferometers, where they significantly improve parameter estimation [11, 12]. For Galactic DWDs, however, the orbital velocities are small ( $\beta < 10^{-2}$ ), and the amplitudes are suppressed by a factor  $\sim \beta$  relative to the quadrupole mode.

From a theoretical perspective, for DWD systems, the mass ratio is the critical parameter for the stability of Roche-lobe overflow and thus closely related to whether a system undergoes a merger or evolves into a long-lived AM CVn binary [e.g. 13]. At the population level, the mass asymmetry distribution provides a key diagnostic of DWD formation channels [6]. The detection of higher harmonics enables a direct measurement of the mass asymmetry and thereby provides observational access to these aspects.

Recently, Ref. [14] presented the first explicit study of PN harmonics from DWDs and showed that they might become observable with LISA in favorable cases. By hypothetically placing two representative systems (HM Cnc

and ZTF J1539 [15]) at different distances, that study examined the prospects for detection with LISA and with the combined LISA–Taiji–TianQin (LTT) network [16–18]. It concluded that while most Galactic DWDs are too weak in their higher harmonics, there remains a non-negligible chance that nearby systems could yield a detection, suggesting that LISA might provide the first glimpse of PN harmonics from DWDs.

The present paper extends Ref. [14] within a systematic and statistical framework. Rather than focusing on a few known binaries, we construct a synthetic Galactic population by sampling masses, frequencies, inclinations, and spatial locations. This enables us to evaluate the detectability of PN harmonics in a more realistic setting. We further extend the analysis to future decihertz observatories such as DECIGO [19] and BBO [20], whose improved sensitivity in the  $\sim 0.01$ – $0.1$  Hz range allows them to detect higher harmonics from hundreds of systems. While LISA will provide the quadrupole detections necessary for a Galactic census, decihertz observatories will capitalize on this foundation by extracting mass-ratio information from the higher harmonics. Together, these missions establish a sequential observational path for space-based gravitational-wave astronomy, extending coverage from the millihertz to the decihertz regime.

The remainder of this paper is organized as follows. In Sec. II we introduce the waveform model including the higher harmonics appearing at 0.5PN order. Sec. III presents the construction of the synthetic population. In Sec. IV we evaluate the detectability of the harmonics with LISA and DECIGO. Sec. V discusses the astrophysical implications and synergies with electromagnetic observations. Finally, Sec. VI provides our main conclusions.

## II. SIGNAL MODEL

### A. Waveform

We consider quasi-circular DWDs with component masses  $m_a, m_b$  ( $m_a > m_b$ ), total mass  $M = m_a + m_b$ , symmetric mass ratio  $\eta = m_a m_b / M^2$ , and chirp mass

$\mathcal{M} = M \eta^{3/5}$ . We also define the fractional mass as difference

$$\Delta = \frac{m_a - m_b}{M}. \quad (1)$$

The orbital frequency is  $f_{\text{orb}}$ , and the gravitational-wave (GW) harmonics are  $f_k = k f_{\text{orb}}$ , with the fundamental ( $k = 2$ ) harmonic at  $f_2 = 2 f_{\text{orb}}$ . In this paper we refer to  $k = 1, 2, 3$  as the *first*, *fundamental*, and *third* harmonics, respectively; when referring to  $\{k = 1, 3\}$  collectively, we use the term *odd harmonics*.

We introduce the post-Newtonian (PN) velocity parameter,  $\beta \sim v/c$ , defined by

$$\begin{aligned} \beta &\equiv \left( \frac{\pi G M f_2}{c^3} \right)^{1/3}, \\ &\simeq 5.37 \times 10^{-3} \left( \frac{M}{M_{\odot}} \right)^{1/3} \left( \frac{f_2}{10 \text{ mHz}} \right)^{1/3}. \end{aligned} \quad (2)$$

At 0.5PN order, the two polarizations in the principal polarization frame take the form [8–10] as

$$\begin{aligned} h_+(t) &= A \left[ a_{2,+}(I) \cos(2\Psi) \right. \\ &\quad \left. + \beta \Delta (a_{1,+}(I) \cos \Psi + a_{3,+}(I) \cos(3\Psi)) \right], \end{aligned} \quad (3)$$

$$\begin{aligned} h_{\times}(t) &= A \left[ a_{2,\times}(I) \sin(2\Psi) \right. \\ &\quad \left. + \beta \Delta (a_{1,\times}(I) \sin \Psi + a_{3,\times}(I) \sin(3\Psi)) \right]. \end{aligned} \quad (4)$$

where

$$A = \frac{2(G\mathcal{M})^{5/3}(\pi f_2)^{2/3}}{c^4 d} \quad (5)$$

is the leading-order quadrupole amplitude at distance  $d$ ,  $\Psi$  is the orbital phase with  $\dot{\Psi} = 2\pi f_{\text{orb}}$ , and  $I$  is the inclination.

The angular coefficients  $a_{k,\{+,\times\}}(I)$  are

$$a_{2,+}(I) = -(1 + \cos^2 I), \quad a_{2,\times}(I) = -2 \cos I, \quad (6)$$

$$a_{1,+}(I) = -\frac{\sin I}{8} (5 + \cos^2 I), \quad a_{1,\times}(I) = -\frac{3}{4} \sin I \cos I, \quad (7)$$

$$a_{3,+}(I) = +\frac{9}{8} \sin I (1 + \cos^2 I), \quad a_{3,\times}(I) = +\frac{9}{4} \sin I \cos I. \quad (8)$$

In Eqs. (3) and (4), the fundamental mode with phase  $2\Psi$  provides the dominant signal, while the first and third harmonics with phases  $\Psi$  and  $3\Psi$  appear only at 0.5PN order and scale as  $\propto \beta \Delta$ . They vanish in the equal-mass limit  $\Delta = 0$  and therefore provide a direct probe of mass asymmetry.

For convenience, we define the geometrical factor

$$E_k(I) \equiv \sqrt{a_{k,+}^2(I) + a_{k,\times}^2(I)}, \quad (9)$$

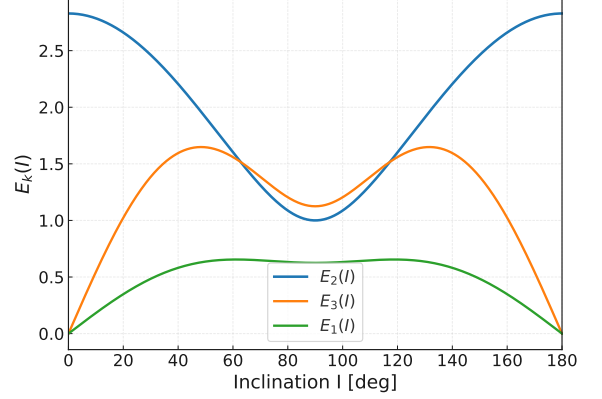


FIG. 1. Inclination dependence of the geometrical factors  $E_k(I) = \sqrt{a_{k,+}^2 + a_{k,\times}^2}$  for  $k = 1, 2, 3$ . The odd-harmonic factors vanish for face-on configurations ( $I = 0$  or  $\pi$ ).

which characterizes the effective angular strength of each harmonic  $k$ . Figure 1 shows  $E_k(I)$  for  $k = 1, 2, 3$ ; the odd-harmonic factors vanish for face-on configurations ( $I = 0, \pi$ ). We also have

$$\frac{E_3(I)}{E_2(I)} = \frac{9}{8} \sin I, \quad (10)$$

and

$$\frac{1}{3} \leq \frac{E_1(I)}{E_3(I)} \leq \frac{5}{9}. \quad (11)$$

The overall scaling of the odd-harmonic amplitude is  $A \beta \Delta$ . At fixed  $M$ , we write  $m_a = M(1 + \Delta)/2$  and  $m_b = M(1 - \Delta)/2$ , which gives  $\eta = (1 - \Delta^2)/4$ . Since  $A \propto \mathcal{M}^{5/3} \propto \eta$  (for fixed  $M, f_2, d$ ) and  $\beta \propto M^{1/3}$  is independent of  $\Delta$ , we obtain

$$A \beta \Delta \propto \frac{\Delta(1 - \Delta^2)}{4}, \quad (12)$$

which is maximized at  $\Delta = 1/\sqrt{3} \simeq 0.58$ , corresponding to a moderately asymmetric binary ( $m_a : m_b \simeq 3 : 1$ ).

In addition to the first and third harmonics arising at 0.5PN order, further contributions exist from eccentricity-induced harmonics and from the 1PN corrections. The former have already been discussed in detail elsewhere [14] and are not repeated in this paper. The latter scale as  $\beta^2$  and are therefore expected to be far weaker than the 0.5PN harmonics considered here. A quantitative assessment of their impact is deferred to Sec. IV.

## B. Signal-to-noise ratios

The response of a detector to the incoming waveforms (3) and (4) also depends on the sky position and polar-

ization angle. For LISA-like orbital configurations, however, it is well approximated by the sky- and polarization-averaged response [21]. For an integration time that is an integer multiple of one year, the minimum response to an arbitrary linear polarization is 0.89 times the root-mean-square value [21, 22]. In the following we adopt this averaged treatment, retaining only the inclination dependence through  $E_k(I)$  [23].

For a quasi-monochromatic source integrated over time  $T$ , the per-harmonic SNRs in a single LISA-like unit are given by [24]

$$\rho_2 \simeq \frac{AE_2(I)}{\sqrt{S_n(f_2)}}\sqrt{T}, \quad (13)$$

$$\rho_3 \simeq \frac{A\beta\Delta E_3(I)}{\sqrt{S_n(f_3)}}\sqrt{T}, \quad (14)$$

$$\rho_1 \simeq \frac{A\beta\Delta E_1(I)}{\sqrt{S_n(f_1)}}\sqrt{T}. \quad (15)$$

Here  $S_n(f) = S_{\text{inst}}(f) + S_{\text{exgal}}(f)$  is the angle-averaged noise power spectral density, consisting of the instrumental part  $S_{\text{inst}}(f)$  and the extra-galactic white-dwarf confusion foreground  $S_{\text{exgal}}(f)$ . Galactic confusion noise from unresolved binaries is not included, since our analysis is restricted to binaries with  $f_2 \gtrsim 5$  mHz, where such systems are expected to be individually resolved by LISA.

For  $S_{\text{inst}}(f)$  we adopt the analytic form of [24] for LISA, those of [25, 26] for Taiji and TianQin, and the formulas in [21] for DECIGO and BBO. Based on [27], we fit the extra-galactic DWD foreground around 1–60 mHz by

$$S_{\text{exgal}}(f) = \left[0.5 \times 10^{a+bu+cu^2}\right]^2, \quad (16)$$

with  $u = \log_{10}(f/10^{-2} \text{ Hz})$  and  $(a, b, c) = (-20.523, -1.847, -0.722)$ . The prefactor 0.5 corresponds to the pessimistic scaling discussed in [27].

Figure 2 illustrates the adopted noise spectra. Around 10 mHz, LISA, Taiji, and TianQin show relatively weak frequency dependence in their sensitivities, dominated by position noise ( $\propto f^0$ ). In contrast, for DECIGO and BBO the sensitivity is dominated by the extra-galactic foreground, producing a much sharper frequency dependence. This distinction is crucial for evaluating the detectability of higher harmonics at  $f \gtrsim 10$  mHz.

The nominal designs of DECIGO and BBO include four units [19]. Two of them are co-located at the same site and therefore do not provide independent noise realizations. The remaining three units are separated by light-travel times of order  $10^3$  s, sufficient to regard their confusion noises as uncorrelated around 10 mHz [28]. Throughout this work we therefore take the effective number of independent detectors to be three, and consistently use the effective sensitivity  $S_n(f)/3$ .

In this paper, we adopt  $\rho_k = 5$  as a conservative working threshold for higher harmonics ( $k = 1, 3$ ). In contrast

to blind searches, which typically require higher thresholds (e.g., close to 7 [29]), the present search is a targeted analysis, once the dominant quadrupole mode is identified and most of the source parameters are tightly constrained.

### III. POPULATION SETUP

In this section we describe the construction of the DWD sample used in our analysis, following the scheme of [30]. Because the total number of Galactic DWDs in the relevant frequency range is subject to astrophysical uncertainties, our analysis primarily emphasizes fractions of systems rather than absolute source counts. To this end, we construct a representative Monte Carlo population of 4000 binaries, which serves as a parent sample for the subsequent analysis.

More specifically, we generate a steady-state population by injecting inspiraling DWDs at  $f_{2,\min} = 4$  mHz, corresponding to the flux of binaries that enter the band, and then evolve them under gravitational radiation reaction. Our focus is restricted to the inspiral phase. Detached systems lose orbital angular momentum mainly through gravitational radiation and gradually inspiral until the less massive component fills its Roche lobe. At that point mass transfer begins, and the subsequent evolution depends on the stability of the transfer [31]: if unstable the binary merges, whereas if stable it enters an outspiral phase [6]. Since the physics of mass-transfer stability remains uncertain (see, e.g., [32, 33]), we restrict our attention to the pre-contact inspiral regime, which is well described by gravitational radiation reaction. This restriction is further justified by the fact that GW amplitude measurements, unlike phase evolution, are not directly linked to the sign of  $f$ .

In Sec. III A we discuss the distribution of component masses. In Sec. III B we specify the assignment of orbital frequencies, and in Sec. III C we introduce the Galactic spatial distribution of DWDs. This framework provides the baseline sample from which signal-to-noise ratios and detection statistics are evaluated in the following sections.

#### A. Binary injection

We inject inspiraling DWDs at  $f_{2,\min} = 4$  mHz, representing the inflow of systems into the observational band, and then draw their component masses  $m_a$  and  $m_b$  independently from the same one-body distribution  $P(m)$ . We order them such that  $m_b < m_a$ . This choice implicitly determines the distribution of mass ratios without introducing it as an explicit parameter.

We approximate the one-body distribution  $P(m)$  by a two-component Gaussian mixture with peaks at  $0.24 M_\odot$  and  $0.64 M_\odot$  (representing typical He and CO white

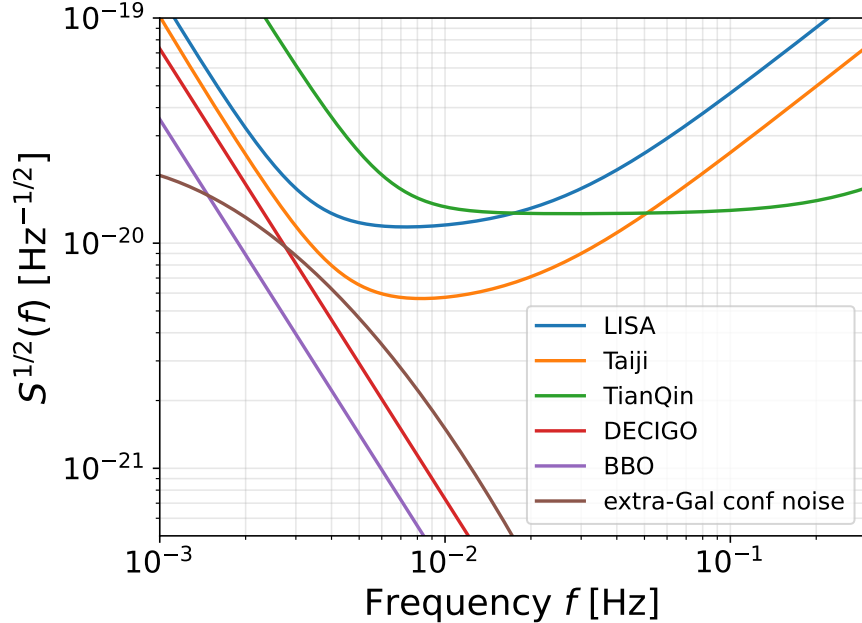


FIG. 2. Adopted noise spectra for space-based detectors. The curves show the instrumental terms  $S_{\text{inst}}(f)$  (LISA, Taiji, TianQin, DECIGO, BBO) and the extra-galactic white-dwarf foreground  $S_{\text{exgal}}(f)$  from Eq. (16). The vertical axis shows  $\sqrt{S(f)}$  (Hz $^{-1/2}$ ), where  $S(f)$  denotes the respective spectra. The figure displays  $S_{\text{inst}}$  and  $S_{\text{exgal}}$  separately; it does not show the summed  $S_n = S_{\text{inst}} + S_{\text{exgal}}$  nor the  $S_n/3$  scaling used for the three independent DECIGO/BBO units.

dwarfs), with relative fractions of 0.55 and 0.45, respectively (see, e.g., [34] for a recent observational study). The support is restricted to  $0.11\text{--}1.1 M_{\odot}$ , and  $P(m)$  is normalized to unity over this interval.

The instantaneous (snapshot) mass distribution is biased toward long-lived systems. In the inspiral phase the quadrupole frequency evolves as

$$\dot{f}_2 \propto \mathcal{M}^{5/3} f_2^{11/3}, \quad (17)$$

where  $\mathcal{M}$  is the chirp mass (ignoring the finite size effects). The corresponding residence time in a frequency band scales approximately as  $\mathcal{M}^{-5/3}$ . Thus, our snapshot-level mass distribution is given by

$$p_{\text{snap}}(m_a, m_b) \propto \mathcal{M}^{-5/3} P(m_a) P(m_b). \quad (18)$$

### B. Frequency assignment

We set the upper edge of the inspiral band at the onset of mass transfer from the donor, when its radius becomes equal to the Roche-lobe radius  $R_L$ . For simplicity we adopt the approximate scaling of [31],

$$R_L \simeq 23^{-4/3} a m_b^{1/3} (m_a + m_b)^{-1/3}, \quad (19)$$

where  $a$  is the orbital separation. For the donor radius we use the analytic expression for a completely degenerate white dwarf given in Verbunt & Rappaport [35], multiplied by an inflation factor  $\eta_R = 1.2$  to allow for possible radius expansion [36]

The corresponding binary separation  $a_{\text{RL}}(m_a, m_b)$  then yields the limiting quadrupole frequency

$$f_{2,\text{RL}}(m_a, m_b) = \frac{1}{\pi} \left[ \frac{G(m_a + m_b)}{a_{\text{RL}}^3} \right]^{1/2}. \quad (20)$$

Given a binary with component masses  $(m_a, m_b)$ , we assign its GW frequency by assuming a steady-state inspiral driven by radiation reaction, for which  $dN/df_2 \propto f_2^{-11/3}$ . We therefore draw  $f_2$  from the interval

$$f_2 \in [f_{2,\text{min}}, f_{2,\text{RL}}(m_a, m_b)], \quad (21)$$

where the lower cutoff is fixed at the injection frequency  $f_{2,\text{min}} = 4$  mHz. The normalized probability density is then

$$p_{\text{inj}}(f_2 | m_a, m_b) = \frac{8}{3} \frac{f_2^{-11/3}}{f_{2,\text{min}}^{-8/3} - f_{2,\text{RL}}(m_a, m_b)^{-8/3}}. \quad (22)$$

In the subsequent analysis, we restrict the working sample to  $f_2 \gtrsim 5$  mHz to focus on a clean regime where Galactic binaries are safely resolvable and less affected by our artificial injection frequency of 4mHz. As demonstrated below, the qualitative conclusions are not sensitive to modest variations of this threshold frequency.

Out of 4000 binaries injected at  $f_{2,\text{min}} = 4$  mHz, a total of 1858 systems evolve to  $f_2 \geq 5$  mHz. These constitute the working sample used throughout this paper. The corresponding frequency distribution is shown in Fig. 3.

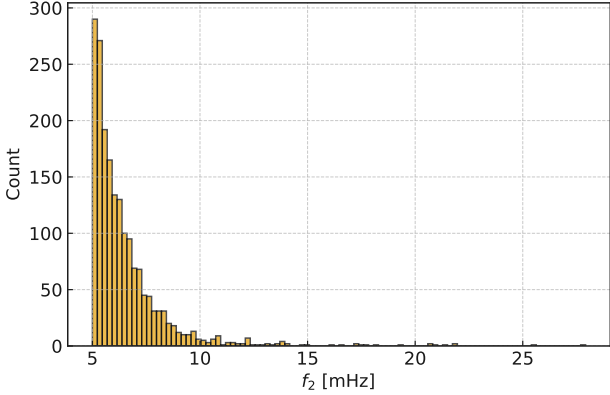


FIG. 3. Histogram of quadrupole GW frequencies  $f_2$  for the 1858 binaries with  $f_2 \geq 5$  mHz in the analysis sample.

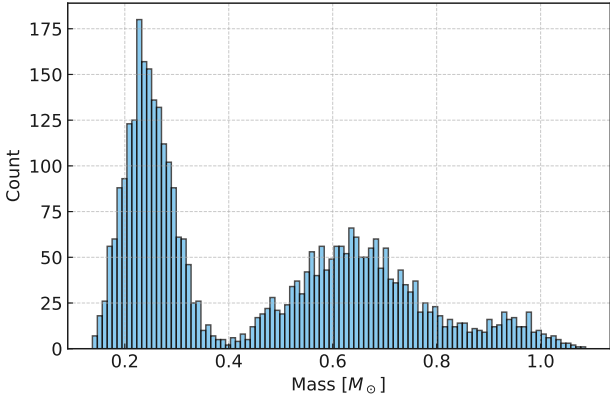


FIG. 4. Histogram of component masses for the 1858 binaries. Distinct peaks correspond to He and CO white dwarfs, with a high-mass tail associated with the CO component.

The sample contains 73 systems at  $f_2 \geq 10$  mHz and 16 systems at  $f_2 \geq 15$  mHz.

In addition, Fig. 4 shows the component-mass distribution for the same set of 1858 DWDs (3716 white dwarfs in total). The He and CO peaks are clearly visible, together with a small high-mass tail associated with the CO component.

### C. Galactic distribution

We next describe the spatial distribution of Galactic close DWDs, modeled as an axisymmetric thin disk plus a spherical bulge component [3]. We place the observer at  $(R_0, \phi, z) = (8.3 \text{ kpc}, 0, 0)$  in Galactocentric cylindrical coordinates.

The normalized source density is written as

$$n(R, z) = (1 - f_{\text{bulge}}) n_{\text{disk}}(R, z) + f_{\text{bulge}} n_{\text{bulge}}(r), \quad (23)$$

where  $n_{\text{disk}}$  and  $n_{\text{bulge}}$  are each normalized to unity,  $f_{\text{bulge}}$

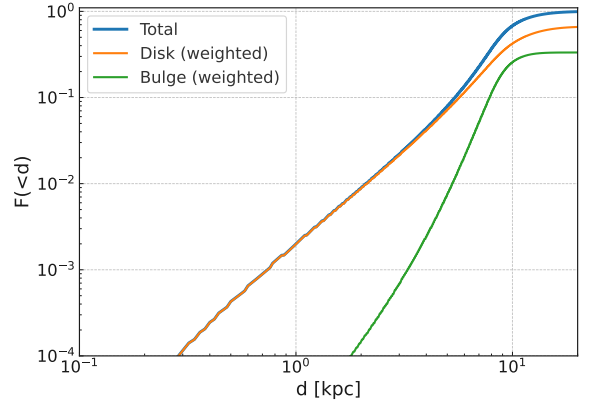


FIG. 5. Cumulative distribution of heliocentric distances  $F(< d)$  for the disk, bulge, and total populations defined in Eq. (27).

denotes the adopted bulge fraction, and  $r = \sqrt{R^2 + z^2}$ . We set  $f_{\text{bulge}} = 1/3$ .

The disk profile is modeled by a double exponential,

$$n_{\text{disk}}(R, z) = \frac{1}{4\pi R_d^2 z_d} \exp\left(-\frac{R}{R_d}\right) \exp\left(-\frac{|z|}{z_d}\right), \quad (24)$$

and the bulge by a spherical exponential,

$$n_{\text{bulge}}(r) = \frac{1}{8\pi R_b^3} \exp\left(-\frac{r}{R_b}\right). \quad (25)$$

We adopt  $R_d = 2.5$  kpc for the disk radial scale length,  $z_d = 0.2$  kpc for the vertical scale height, and  $R_b = 1.0$  kpc for the bulge scale length.

The heliocentric distance to a point  $(R, \phi, z)$  is

$$d(R, \phi, z) = \sqrt{R^2 + R_0^2 - 2RR_0 \cos \phi + z^2}, \quad (26)$$

and the cumulative distribution of source distances is

$$F(< d) = \int_{d(R, \phi, z) \leq d} n(R, z) R dR d\phi dz. \quad (27)$$

Figure 5 shows the cumulative distribution. At small distances ( $d \lesssim 0.5$  kpc), the cumulative distribution approximately follows  $F(< d) \propto d^{2.5}$ , reflecting the local geometry of the thin disk [14]. The nearby population is dominated by the disk, while the bulge contribution becomes significant only toward the Galactic center. At larger radii the disk again dominates, and nearly all Galactic DWDs are contained within  $d < 20$  kpc in this model.

The binary inclination  $I$  is assumed to be isotropic, with  $\cos I$  uniformly distributed in  $[-1, 1]$ .

### IV. OBSERVATIONAL IMPACT

In this section we quantify the detection prospects for different harmonics of the GW signal from Galactic DWDs. Our aim is to clarify the successive stages

TABLE I. Number of binaries with  $\rho_k > 5$  for each harmonic ( $k = 1, 2, 3$ ) and detector configuration. The analysis sample contains 1858 systems at  $f_2 \geq 5$  mHz. LTT denotes the LISA–Taiji–TianQin network.

Harmonic	LISA (4yr)	LTT (4yr)	DECIGO (10yr)	BBO (10yr)
$\rho_1$	0	0	1	1
$\rho_2$	1857	1858	1858	1858
$\rho_3$	0	1	135	170

of observation, beginning with LISA-class detectors and extending to future decihertz observatories. We first present overall detection counts, then examine the quadrupole baseline, turn to the odd harmonics, and finally study their dependence on distance and frequency before closing with a brief summary.

### A. Overview

LISA (and the LISA–Taiji–TianQin (LTT) network) can detect the fundamental quadrupole mode with high confidence, providing an initial inventory of nearly monochromatic Galactic binaries. DECIGO and BBO, with superior sensitivity in the 0.01–0.1 Hz band, can probe the higher harmonics. Since their effective sensitivities are limited by the extra-galactic confusion foreground, DECIGO and BBO yield similar performance (see Fig. 2), and we mainly present results for DECIGO in what follows. The potential role of the LTT network in enabling the first detection of the third harmonic was previously noted by [14], but its impact on the systematic study presented here is very limited.

Table I summarizes the number of binaries with  $\rho_k > 5$  (the SNR of the  $k$ th harmonic) across representative detectors.

### B. Quadrupole performance

Figure 6 shows the detection fraction of the quadrupole harmonic ( $\rho_2$ ) as a function of the SNR threshold. For the LISA mission with a 4 yr observation time, nearly all of the 1858 binaries lie above the threshold. The minimum quadrupole SNR is  $\rho_2 \simeq 4.7$ . Only one system has  $\rho_2 \leq 5$ , and only three systems have  $\rho_2 \leq 7$  among the 1858 binaries considered. Thus, even adopting a higher threshold of  $\rho_2 = 7$  for blind searches, LISA would still robustly detect the fundamental modes for essentially the entire Galactic DWD population in this frequency range.

The distribution extends up to  $\rho_2 \simeq 2200$ , demonstrating a wide dynamic range. This demonstrates that LISA can robustly detect virtually all Galactic DWDs in this frequency range, consistent with the long-standing conclusion that LISA will provide a nearly complete census of the population for  $f_2 \gtrsim 4$  mHz [6].

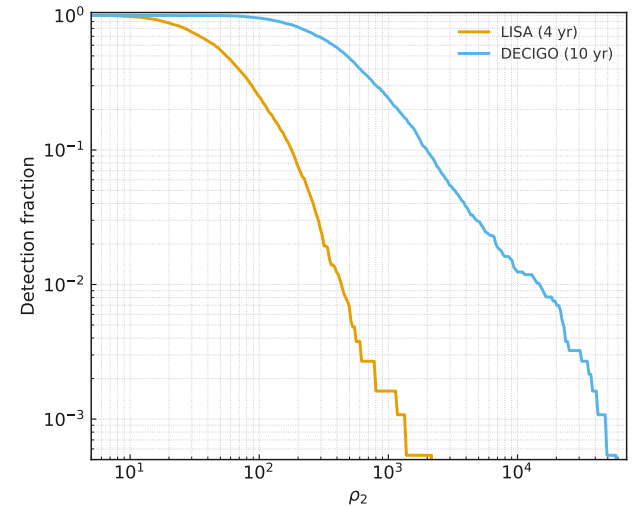


FIG. 6. Detection fraction of the quadrupole harmonic ( $\rho_2$ ) as a function of the SNR threshold for LISA (orange) and DECIGO (blue).

For DECIGO, operating with a 10 yr mission, the sensitivity is even higher. The weakest source in our sample still has  $\rho_2 \simeq 31$ , while the strongest reaches  $\rho_2 \simeq 5.9 \times 10^4$ . Thus the detection is guaranteed with ample margin.

### C. Odd harmonics

Figure 7 shows the detection fractions for the first ( $\rho_1$ ) and third ( $\rho_3$ ) harmonics as a function of the SNR threshold. For LISA, the odd harmonics are effectively inaccessible: no systems exceed SNR = 5 for either  $\rho_1$  or  $\rho_3$ , and only a single case appears in the LTT configuration (4 yr). As discussed in [14], rare nearby binaries might yield detectable odd harmonics even with LISA, but such cases would be exceptional rather than representative. LISA is therefore unlikely to provide a systematic view of the odd harmonics.

For DECIGO, we explicitly examine how the detectability of the third harmonic depends on the adopted SNR threshold  $\rho_3$ . Figure 7 (right panel) shows the detection fraction as a function of this threshold. Lowering the threshold from the fiducial value  $\rho_3 = 5$  to 4 and 3 increases the number of detectable systems from 135 to 197 and 306, respectively, in our sample of 1858 binaries. Although the absolute detection counts vary, the qualitative trends remain unchanged.

For completeness, we also consider the combined odd-harmonic SNR  $\rho_{\text{odd}} \equiv \sqrt{\rho_1^2 + \rho_3^2}$ . Among the 1858 sources, the number of systems with  $\rho_{\text{odd}} > 5$  is 0 (LISA, 4 yr), 1 (LTT, 4 yr), 137 (DECIGO, 10 yr), and 172 (BBO, 10 yr). Compared with the corresponding counts for the third harmonic alone (0, 1, 135, and 170), the contribution of the first harmonic remains marginal, though

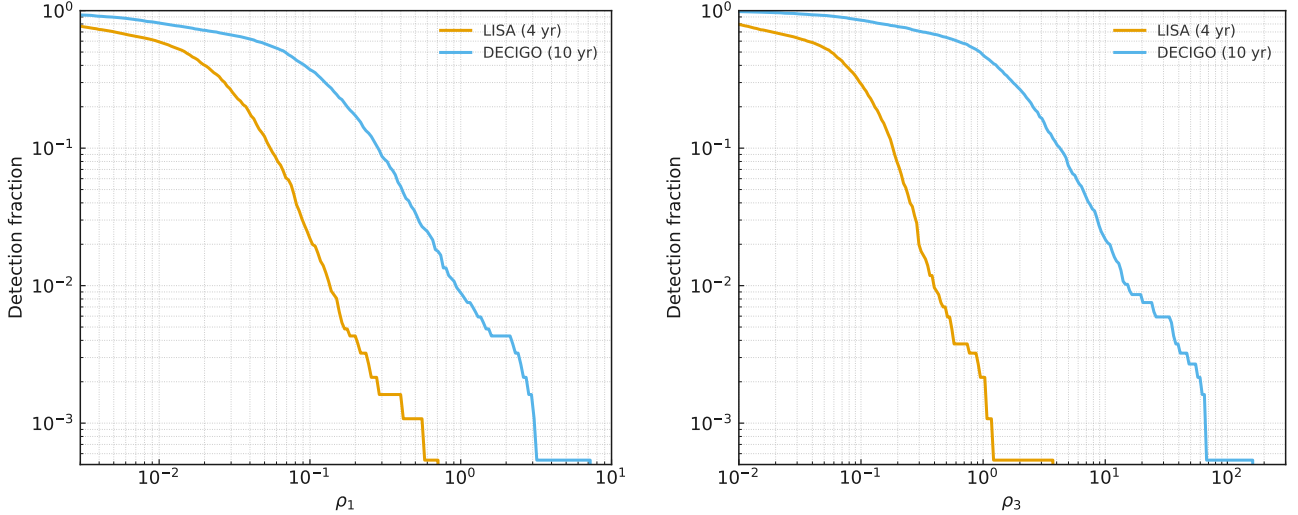


FIG. 7. Detection fraction as a function of the SNR threshold for the first ( $\rho_1$ , left) and third ( $\rho_3$ , right) harmonics, for LISA (orange) and DECIGO (blue).

it can slightly increase the detection statistics for the decihertz observatories.

#### D. Spatial and frequency domains

Figure 8 displays the third-harmonic SNR  $\rho_3$  as functions of distance (left) and quadrupole frequency  $f_2$  (right). The horizontal dashed line indicates the fiducial threshold SNR = 5. In the distance panel, the upper envelope of the DECIGO points follows the expected  $d^{-1}$  scaling of the GW amplitude. The detection fraction decreases gradually with distance: about 56% of systems within 2.5 kpc exceed the threshold, and even in the range 7.5–10 kpc the fraction is still  $\sim 6\%$ . This demonstrates that higher harmonics can be probed throughout the Galaxy with DECIGO. In contrast, the LISA points lie entirely below the threshold line, confirming that only very nearby binaries would be detectable with LISA.

In the frequency panel, the DECIGO results exhibit a steep increase of the third-harmonic SNR  $\rho_3$  with the quadrupole frequency  $f_2$ . This trend reflects both the post-Newtonian scaling  $\beta \propto f_2^{1/3}$  and, more importantly, the rapid decline of the extra-galactic foreground  $S_{\text{Exgal}}(f)$  toward higher frequencies, as shown in Fig. 2.

In our sample population of 1858 binaries at  $f_2 > 5$  mHz, this frequency dependence results in 135 systems exceeding the working threshold  $\rho_3 = 5$ , as mentioned earlier. The detected population is strongly concentrated at the high-frequency end: 122 of these systems have  $f_2 \geq 6$  mHz and 106 have  $f_2 \geq 7$  mHz, while 43 systems reside above  $f_2 = 10$  mHz. Although such high-frequency binaries constitute only a small fraction of the overall population, they contribute a disproportionate share of the detected systems owing to the rapid growth

of  $\rho_3$  with frequency.

This concentration toward higher frequencies indicates that the main conclusions are not sensitive to the precise choice of the lower frequency cut adopted in the analysis.

The vertical spread of points at fixed  $(d, f_2)$  is primarily driven by the mass asymmetry  $\Delta$ , consistent with the  $\rho_3 \propto \Delta$  scaling of higher harmonics, with orientation effects being subdominant.

#### E. Summary

In summary LISA will provide a nearly complete census of Galactic DWDs through detections of the fundamental quadrupole mode at  $f_2 \gtrsim 5$  mHz. Decihertz observatories such as DECIGO and BBO will extend this foundation by detecting higher harmonics, in particular the third mode for hundreds of systems and the first mode only for rare systems. These capabilities together outline a sequential observational strategy, progressing from a secure quadrupole census to detailed multi-harmonic studies in the  $\sim 10$  mHz regime.

It should be emphasized that the absolute detection counts depend to some extent on the assumed population model. Modest changes in the adopted lower-mass distribution lead to variations at the level of several tens of systems, without altering the overall conclusion that the detectable fraction may be on the order of 10%. Further discussion of this dependence is deferred to Sec. V B.

We finally note that harmonics induced by orbital eccentricity, as already noted in Sec. II and discussed in detail by [14], lie beyond the scope of this study. At still higher post-Newtonian order, the amplitudes scale with  $\beta^2$ , and even with the very large quadrupole SNRs achievable by DECIGO ( $\rho_2^{\text{max}} \sim 5.9 \times 10^4$  in our sam-

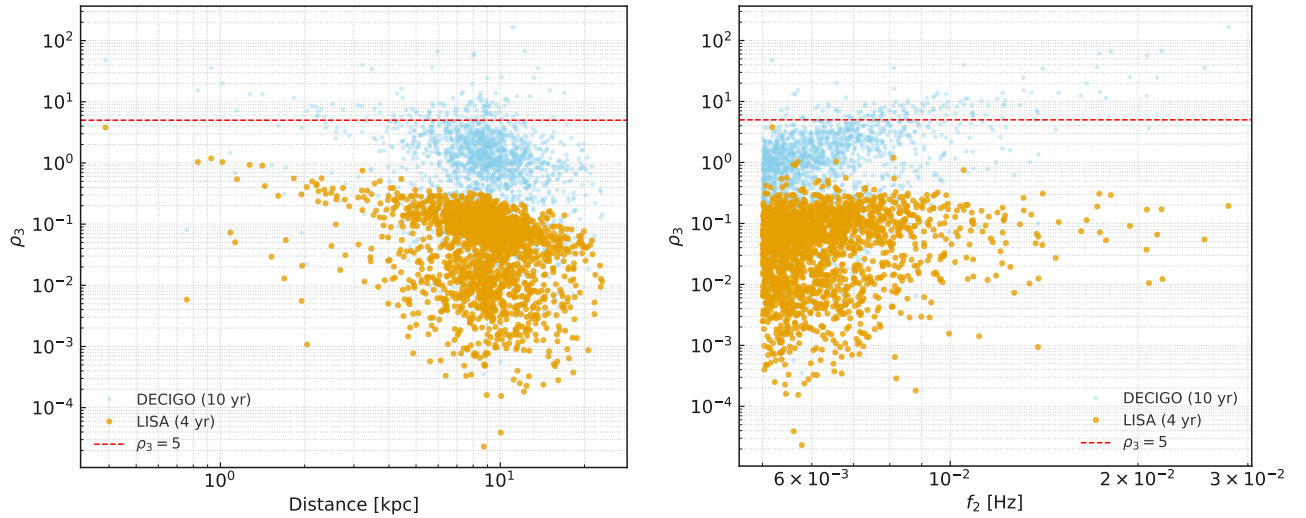


FIG. 8. SNRs of the third harmonic ( $\rho_3$ ) as a function of distance (left) and quadrupole frequency  $f_2$  (right), for LISA (orange) and DECIGO (blue). The horizontal dashed line marks the threshold  $\rho_3 = 5$ .

ple), the corresponding subdominant contributions are expected to remain undetectable in the vast majority of systems.

## V. DISCUSSION AND IMPLICATIONS

In this section, we discuss the broader implications of our results, including combination with electromagnetic observations. We also outline the main limitations of our study and directions for future investigation.

### A. Astrophysical implications and EM synergy

Electromagnetic information, in particular accurate distances, may be combined with GW amplitudes  $A \propto \mathcal{M}^{5/3}/d$  to infer the chirp mass  $\mathcal{M}$ , which is less sensitive to finite-size corrections than chirp-mass estimates based on  $\dot{f}$  [37]. Cross-calibration of these methods would strengthen the robustness of chirp-mass measurements.

When higher harmonics are detected, the mass ratio can be constrained as well, enabling estimates of the two component masses. This is particularly important for AM CVn systems, where electromagnetic observations alone often fail to yield solid constraints on mass ratios, as illustrated by HM Cnc [38, 39]. In such cases, GW harmonics could provide critical insight into binary configuration and evolutionary pathways.

### B. Limitations and future work

Several limitations of our study should be noted. First, we have not attempted to model the outspiral phase

following Roche-lobe overflow, focusing instead on the inspiraling regime. As discussed earlier, the amplitude measurements considered here do not depend directly on the sign of  $\dot{f}$ . However, the quoted fractions (e.g., the  $\sim 10\%$  for the third harmonic) refer specifically to the pre-contact inspiral sample and could differ once post-contact outspiral systems are included.

Second, our injection model is based on simplified distributions of component masses and radii. While this simplified treatment is expected to capture the main features of the observational prospects, the detailed quantitative results depend on the adopted population model. For example, in our baseline configuration ( $f_2 \geq 5$  mHz) the working sample contains 1858 binaries, of which 135 (7.3%) exceed  $\rho_3 > 5$  in DECIGO. Adopting an alternative but still plausible mass distribution (He peak shifted to  $0.25 M_\odot$  and the lower bound raised from  $0.11$  to  $0.12 M_\odot$ ) yields 1897 binaries with 159 detections (8.4%). These variations illustrate that the absolute counts should not be over-interpreted. For the assumptions considered here, the detection fraction is on the order of 10%.

A further caveat concerns the low-frequency sensitivity of DECIGO. In the present study, the noise level around 10 mHz is assumed to be dominated by radiation-pressure noise in Fabry–Perot arm [19]. Because the arm length is relatively short, the technical requirements on the acceleration noise are demanding, and the final sensitivity goal may be less ambitious than in the analytic model adopted here. To assess robustness, we examined the effect of halving the SNRs. Even under this assumption, the third harmonic remains observable in  $\sim 40$  binaries, allowing statistical studies at this level of degradation. Future design work will clarify realistic targets for the low-frequency band.

Our LISA forecasts motivate stacking of sub-threshold

odd harmonics. Such methods should be robust to the four-fold phase ambiguity [40], guided by the quadrupole posterior, and calibrated with permutation tests. A systematic study of weighting schemes and noise robustness is left to future work.

## VI. CONCLUSIONS

We have investigated the detectability of the first and third harmonics from Galactic DWDs around 10 mHz. We conclude that LISA will provide a nearly complete census of the population through detections of the quadrupole mode, while decihertz observatories such as DECIGO and BBO will be able to access higher harmonics in a significant subset of the same systems. In particular, the third harmonic is expected to be measurable for roughly 10% of inspiral binaries with detectable quadrupole emission above 5 mHz. This will enable constraints on the binary mass ratio. Together, these capabilities define a long-term observational strategy for

space-based gravitational-wave astronomy.

While most attention on decihertz observatories has focused on the 0.1–1 Hz range, where the noise floor is expected to be lowest and cosmological signals such as an inflationary background may be probed, our results highlight the importance of the  $\sim$ 10 mHz regime, bridging the observational domains of LISA and DECIGO/BBO. If sensitivities at the level assumed in this work can be realized, this band will not only connect different mission domains but also provide valuable astrophysical insights into the configuration and evolution of compact binaries [e.g., 6, 13].

## ACKNOWLEDGMENTS

The author thanks the participants of the MIAPbP program “Enabling Future Gravitational Wave Astrophysics in the Milli-Hertz Regime” (Munich, 2025) for helpful discussions.

---

- [1] G. Nelemans, S. F. Portegies Zwart, F. Verbunt, and L. R. Yungelson, *Astron. Astrophys.* **368**, 939 (2001), arXiv:astro-ph/0101123.
- [2] A. J. Ruiter, K. Belczynski, M. Benacquista, S. L. Larson, and G. Williams, *Astrophys. J.* **717**, 1006 (2010), arXiv:0705.3272 [astro-ph].
- [3] S. Nissanke, M. Vallisneri, G. Nelemans, and T. A. Prince, *The Astrophysical Journal* **758**, 131 (2012).
- [4] A. Lamberts, S. Blunt, T. B. Littenberg, S. Garrison-Kimmel, T. Kupfer, and R. E. Sanderson, *Mon. Not. Roy. Astron. Soc.* **490**, 5888 (2019), arXiv:1907.00014 [astro-ph.HE].
- [5] V. Korol, N. Hallakoun, S. Toonen, and N. Kärnänen, *Mon. Not. Roy. Astron. Soc.* **511**, 5936 (2022), arXiv:2109.10972 [astro-ph.HE].
- [6] P. A. Seoane *et al.* (LISA), *Living Rev. Rel.* **26**, 2 (2023), arXiv:2203.06016 [gr-qc].
- [7] A. Toubiana, N. Kärnänen, A. Lamberts, and M. C. Miller, arXiv preprint arXiv:2403.16867 (2024).
- [8] L. E. Kidder, *Physical Review D* **52**, 821 (1995).
- [9] L. Blanchet, *Living reviews in relativity* **17**, 2 (2014).
- [10] E. Poisson and C. M. Will, *Gravity: Newtonian, post-newtonian, relativistic* (Cambridge University Press, 2014).
- [11] R. Abbott, T. Abbott, S. Abraham, F. Acernese, K. Ackley, C. Adams, R. X. Adhikari, V. Adya, C. Affeldt, M. Agathos, *et al.*, *Physical Review D* **102**, 043015 (2020).
- [12] R. Abbott, T. Abbott, S. Abraham, F. Acernese, K. Ackley, C. Adams, R. X. Adhikari, V. Adya, C. Affeldt, M. Agathos, *et al.*, *The Astrophysical Journal Letters* **896**, L44 (2020).
- [13] K. A. Postnov and L. R. Yungelson, *Living Reviews in Relativity* **17**, 3 (2014).
- [14] N. Seto, *Phys. Rev. Lett.* **135**, 061402 (2025), arXiv:2506.23441 [astro-ph.HE].
- [15] J. Chakraborty *et al.*, (2024), arXiv:2411.12796 [astro-ph.HE].
- [16] W.-R. Hu and Y.-L. Wu, *The taiji program in space for gravitational wave physics and the nature of gravity* (2017).
- [17] J. Luo, L.-S. Chen, H.-Z. Duan, Y.-G. Gong, S. Hu, J. Ji, Q. Liu, J. Mei, V. Milyukov, M. Sazhin, *et al.*, *Classical and Quantum Gravity* **33**, 035010 (2016).
- [18] R.-G. Cai, Z.-K. Guo, B. Hu, C. Liu, Y. Lu, W.-T. Ni, W.-H. Ruan, N. Seto, G. Wang, and Y.-L. Wu, *Fund. Res.* **4**, 1072 (2024), arXiv:2305.04551 [gr-qc].
- [19] S. Kawamura *et al.*, *Class. Quant. Grav.* **28**, 094011 (2011).
- [20] G. M. Harry, P. Fritschel, D. A. Shaddock, W. Folkner, and E. S. Phinney, *Class. Quant. Grav.* **23**, 4887 (2006), [Erratum: *Class.Quant.Grav.* 23, 7361 (2006)].
- [21] K. Yagi and N. Seto, *Physical Review D* **83**, 044011 (2011).
- [22] N. Seto, *Phys. Rev. D* **69**, 123005 (2004), arXiv:gr-qc/0403014.
- [23] This approximation is not valid for the proposed TianQin orbit.
- [24] T. Robson, N. J. Cornish, and C. Liu, *Class. Quant. Grav.* **36**, 105011 (2019), arXiv:1803.01944 [astro-ph.HE].
- [25] Z. Luo, Z. Guo, G. Jin, Y. Wu, and W. Hu, *Results in Physics* **16**, 102918 (2020).
- [26] J. Mei *et al.* (TianQin), *PTEP* **2021**, 05A107 (2021), arXiv:2008.10332 [gr-qc].
- [27] A. J. Farmer and E. S. Phinney, *Mon. Not. Roy. Astron. Soc.* **346**, 1197 (2003), arXiv:astro-ph/0304393.
- [28] N. Seto, *Phys. Rev. D* **104**, 063025 (2021), arXiv:2108.12930 [gr-qc].
- [29] M. C. Digman and N. J. Cornish, *Astrophys. J.* **940**, 10 (2022).
- [30] N. Seto, *Phys. Rev. Lett.* **128**, 041101 (2022),

arXiv:2201.03685 [astro-ph.HE].

[31] B. Paczyński, *Acta Astronomica* **17**, 287 (1967).

[32] T. R. Marsh, G. Nelemans, and D. Steeghs, *Mon. Not. Roy. Astron. Soc.* **350**, 113 (2004), arXiv:astro-ph/0312577.

[33] V. Gokhale, X. M. Peng, and J. Frank, *Astrophys. J.* **655**, 1010 (2007), arXiv:astro-ph/0610919.

[34] J. Munday, I. Pelisoli, P.-E. Tremblay, D. Jones, G. Nelemans, M. Kilic, T. Cunningham, S. Toonen, A. Santos-García, H. Dawson, V. Pinter, B. Godson, L. Martinez, J. Chand, R. Dobson, K. Jhass, and S. Shenoy, *Mon. Not. Roy. Astron. Soc.* **541**, 3494 (2025), arXiv:2507.14123 [astro-ph.SR].

[35] F. Verbunt and S. Rappaport, *Astrophys. J.* **332**, 193 (1988).

[36] This choice is consistent with the Roche-lobe filling of HM Cnc for  $m_b = 0.17 M_\odot$  at  $f_2 = 6.2$  mHz [39].

[37] S. Y. Lau, K. Yagi, and P. Arras, arXiv preprint arXiv:2409.17418 (2024).

[38] T. Kupfer, V. Korol, S. Shah, G. Nelemans, T. Marsh, G. Ramsay, P. Groot, D. Steeghs, and E. Rossi, *Monthly Notices of the Royal Astronomical Society* **480**, 302 (2018).

[39] J. Munday, T. Marsh, M. Hollands, I. Pelisoli, D. Steeghs, P. Hakala, E. Breedt, A. Brown, V. Dhillon, M. J. Dyer, *et al.*, *Monthly Notices of the Royal Astronomical Society* **518**, 5123 (2023).

[40] N. Seto, *Phys. Rev. D* **111**, 083051 (2025), arXiv:2507.01250 [gr-qc].